J. Appl. Comput. Mech., xx(x) (2026) 1-13
DOI: 10.22055/jacm.2026.48860.5557

ISSN: 2383-4536
jacm.scu.ac.ir

Shahid Chamran University of Ahvaz

Journal of Applied and Computational Mechanics

Research Paper

HAM Analysis for Mixed Convection Darcy Forcheimer Couple Stress Ternary Hybrid Nanofluid Flow Embedded in a Permeable Surface with the Impact of Thermal Radiation

Ali Rehman[1,2], Abdullah Aziz Saad[1], Mustafa Inc[3,4,5], Siti Sabariah Binti Abas[4], K. Sudarmozhi[2]

[1] School of Mechanical Engineering, Universiti Sains Malaysia,14300 Nibong Tebal, Penang, Malaysia
[2] Department of Mathematics, Saveetha School of Engineering, SIMATS, Chennai, Tamil Nadu, India
[3] Department of Mathematics, Firat University, 23119 Elazig, Turkiye
[4] Department of Computer Engineering, Biruni University, 34010 Istanbul, Turkiye
[5] Faculty of Informatics and Computing, Universiti Sultan Zainal Abidin, Campus Besut, 22200 Terengganu, Malaysia

Received October 25 2025; Revised January 31 2026; Accepted for publication February 02 2026.
✉ Corresponding authors: A.A. Saad (azizsaad@usm.my); M. Inc (minc@firat.edu.tr)

Abstract. The paper analyses the mixed convection flow of the Darcy–Forchheimer couple-stress model with a ternary hybrid nanofluid (THNF) over a porous stretching surface using the homotopy analysis method (HAM). The THNF, which comprises a ternary hybrid nanofluid with single-walled carbon nanotubes (SWCNTs), multi-walled carbon nanotubes (MWCNTs), and Silver (Ag) nanoparticles dispersed in blood, is expected to enhance the thermal conductivity and energy transport of the fluid and is suitable for biomedical and energy applications. The governing equations account for the resistance of the porous medium (Darcy–Forchheimer), couple-stress rheology, magnetohydrodynamics (MHD) with thermal radiation, viscous dissipation, Joule heating, and heat generation. It uses similarity transformations to linearise the governing nonlinear partial differential equations (PDEs) into ordinary differential equations (ODEs) and uses the BVPh 2.0 to obtain highly accurate velocity and temperature profiles. The study varied the following parameters: Forchheimer number (Fr), porosity (ε), magnetohydrodynamics (M), radiation (R), Eckert (Ec), Grashof (Gr), Biot (Bi), volume fraction (φ) of the nanoparticles, and heat source (Q). It was observed that Fr and ε reduce velocity by 20-40% due to inertial/porous drag and 30% due to Gr, which is a result of buoyancy. The flow decelerated the most under MHD, increasing skin friction. Increased temperatures correlated with R, Ec, and Q, thereby creating thicker thermal boundary layers. The Nusselt number (Nu) due to the synergy between blood and THNF increased by 15-25%. This is due to the absorption of blood THNFs (k_{thnf}) and R. Increased Bi increased the convective heat transfer. Skin friction increased with φ (due to the viscosity enhancement) and Fr (around 20-30% over Fr = 0.2-0.8), then decreased with Gr due to boundary layer reduction. Findings optimise THNF perfusion in vascular scaffolds (thrombosis control via drag/MHD), hyperthermia therapy (localised heating), and porous heat exchangers (compact cooling). HAM convergence ($h_\varphi = -0.9$, $h_\theta = -1.0$) ensures dependability, yielding parametric domains that produce 10-20% excess performance over mono nanofluids.

Keywords: Mixed convection flow, HAM, Darcy–Forchheimer couple-stress model, MHD, thermal radiation, Hybrid nanofluid.

1. Introduction

A hybrid nanofluid (HNF) is a non-Newtonian nanofluid with superior thermal and rheological properties due to the occurrence of two different nanoparticle types in a base fluid, which is non-Newtonian. These fluids are used in industrial, biomedical, energy, and cooling applications where traditional heat-transfer methods are ineffective. Compared to Newtonian fluids, non-Newtonian fluids have a time-, stress-, or shear-rate-dependent viscosity. They have been widely explored in science and engineering because they have been seen to provide superior heat transfer and versatile rheological behaviour. These engineered fluids have been proposed as promising candidates for use in high-performance thermal systems due to their increased thermal conductivity and energy transfer efficiency, as well as improved suspension stability. The synergy between dissimilar nanoparticles in HNFs has enhanced their potential, as they exhibit improved thermal and flow properties, long-term dispersion stability, adjustable viscosity, and enhanced energy transport efficiency, making them applicable to various industrial and technological applications.

Their behaviour has been observed in various recent studies conducted under varying flow and heat transfer conditions. Farooq et al. [1] atomically assessed the HNFs deployed on a stretched sheet by the heat-transfer enhancement regulation. Still, the model did not account for the impact of viscous dissipation and nanoparticle aggregation, which can diminish its accuracy under realistic operating conditions. Farooq et al. [2] used the Cattaneo Christov heat and mass flux theory to examine bio-convective HNF flow of

Published online: February 20 2026

microorganisms in a cylinder. Although informative, they were formulated only under steady-state conditions, not under transient conditions, which limits their application to dynamic systems. Farooq et al. [3] also examined the thermal performance of MWCNT, CuO and SWCNT. Fe_3O_4 HNFs in the stretched cylinder using the response surface methodology. The study simplified the interaction between nanoparticles, although it was effective in optimising the process. However, the computational results were not experimentally verified, raising doubts about their practical applicability. Fiza et al. [4] inspected the 3D MHD rotating nanofluid viscometric flow between porous parallel plates. Still, in their study, the nanoparticle distribution was uniform, and the potential instability caused by secondaries (resulting from rotation) was not considered, which could affect the actual system behaviour.

Lastly, Aaiza et al. [5] examined mixed-convection MHD nanofluid nanoparticle flow with different morphologies in a porous channel, and emphasised the effect of particle shape on energy transfer. However, the experiment failed to account for hybrid nanoparticle suspensions and fixed their thermophysical characteristics, which could not capture nonlinear changes in viscosity and conductivity. Abas et al. [6] calculated the flow of second-order slip micropolar MHD HNF across a stretched surface in the occurrence of a constant activation energy source and a heat source. Their paper was informative regarding the effects of slips and the micropolar nature; however, the analysis was limited to two-dimensional steady-state conditions, nanoparticle aggregation, and non-uniform heating. The analysis only applies to the avenue of real industrial processes. The case of Akbar et al. [7] examines the flow of nanofluids through a rotating disc using the Buongiorno model with partial slip and MHD effects, applied via an intelligent computing paradigm. The computational framework still enhanced predictive accuracy. Still, the HNF suspensions were not considered, and the model strongly depended on idealised boundary conditions that cannot fully capture the complex experimental dynamics.

Akbar et al. [8] also employed neural networks to explore MHD and energy transfer in a two-phase thermal radiation nanofluid flow model. This method effectively demonstrated the integration of machine learning into fluid mechanics; however, the research was limited to the dependence on the training data and was not experimentally validated, so its applicability to real systems remains unclear. Aziz et al. [9] also conducted computational studies of THNF flow with thermal conduction and heat source-sink effects on a stretching surface. Their outcome complemented the knowledge on the complex three-component suspension. Still, the research was limited to the laminar flow regime and did not include the turbulent regime, which is predominant in practical systems. Chu et al. [10] measured the unsteady HNF flow in between two infinite parallel plates by looking into the effects of particle shape in magnetohydrodynamics through a model-based analysis. Although they emphasised the role of nanoparticle morphology, the geometry was simplified by assuming infinite plates, and Brownian motion and thermophoresis were ignored, making the model less realistic.

Lastly, Bilal et al. [11] employed the Levenberg-Marquardt backpropagation technique to compute the unsteady compressing flow between parallel plates with mass and heat exchange. Computational efficiency was achieved through machine learning-based analysis. Still, it did not account for hybrid nanoparticles and transient instabilities in high-Reynolds-number flows, limiting its broader applicability. Giri et al. [12] used the HPM to study the flow of Darcy-Forchheimer nanofluids past a Riga plate. Although this approach was practical for showing the effects of porous media and electromagnetic forcing, the analysis was limited to small perturbations and failed to resolve nonlinearities at high Darcy-Forchheimer parameters. Hussanan et al. [13] observed the MHD free convection in an unsteady boundary layer under Newtonian heating and constant mass diffusion across a porous medium. Their development provided a clear understanding of the heat-mass transfer coupling; however, the assumption of continuous properties and the neglect of HNF suspensions limited their applicability. Imran et al. [14] studied numerically the heat conduction in cross-nanofluid bioconvection flow around a cylinder in the occurrence of melting and swimming microorganisms.

Despite improved knowledge of microorganism-induced transport, the model was not experimentally validated, and hybrid interactions among nanoparticles were not investigated. Khan et al. [15] evaluated MoS_2/SiO_2 HNFs under the inspiration of nonlinear radiation and reported an increase in the heat transfer of a moderately ionised liquid. Although they worked, their model did not account for particle clustering and stability issues, which could have a profound impact on thermal conductivity. Mishra et al. [16] compared MoS_2 -SiO_2 -H_2O hybrid and MoS_2 -SiO_2 -GO/H_2O THNFs under an inclined cylinder, which was heated and absorbed. Although the authors emphasised the superior performance of ternary nanofluids, the results were analysed only in laminar flow, and the potential influence of turbulence under industrial conditions was disregarded. Raja et al. [17] deliberate the flow of micropolar nanofluid through a spinning disc, which is partially slip, and in the occurrence of a magnetic field, using a predictive neuro-computing technique. Their model enhanced predictive performance, but it was limited by the need for training data and the lack of physical validation.

Sheikholeslami et al. [18] numerically simulated a solar thermal system with an HNF, thereby making the tabulator design novel and enhancing the collectors' efficiency. The research, however, failed to capture the long-term stability and fouling of nanoparticles in the solar system. Shoaib et al. [19] combined artificial neural networks and stochastic numerical methods to investigate energy transfer in a Maxwell nanofluid flow over a moving vertical surface in the presence of MHD effects. Although they were computationally innovative, they were computationally expensive and did not cover hybrid nanoparticle suspensions. Ullah et al. [20] studied the THNF flow under radiation and the effect of activation energy. Although they focused on activation energy, their study had a limitation in practical applicability because they assumed a homogeneous nanoparticle distribution and that all thermophysical properties were identical.

The research conducted by Yaseen et al. [21] focused on MoS_2-SiO_2/water HNF flow over convex/concave variable-thickness sheets under ohmic heating and viscous dissipation. The geometric complexity was observed to make the study meaningful, but only the curvatures of specific sheets were considered, which narrowed the scope of the conclusions. Ullah et al. [22] used soft computing techniques to determine the nanofluid energy and mass transfer in an MHD boundary layer over a perpendicular cone under convective boundary conditions. They also provided greater accuracy in their solutions, but the paper did not test hybrid nanoparticle suspensions or compare the results with experiments. Ullah et al. [23] furthered the research on Hall current effects and MHD phenomena in the micro-polar nanofluid flow between two parallel spinning plates in neuro-computing. Although their model was effective in solving nonlinear equations, some shortcomings arose from the utilisation of data-driven methods and the lack of multiparticle or hybrid effects.

Hussain et al. [24] used machine learning to predict the thermal behaviour of a nano-enhanced PCM under double-diffusive convection in lid-driven cavities and around a satellite body with a square heater. The study is limited in that it has only one experimental cavity configuration and no experimental validation to support real-world applicability, although the AI-supported framework's predictive capability improved. The fin-assisted NEPCM-filled enclosure with MHD and radiative convection under combined thermal and solutal gradients was studied by Hussain et al. [25], and improved the cooling and energy storage. The analysis, however, assumes constant thermal physical properties and ignores phase-change hysteresis, so it is unclear what the net impact on the system's reliability is.

Hussain et al. [26] enhanced heat transfer through microorganism-induced mixing of a finned complex cavity containing nano-enhanced PCM and oxytactic microorganisms in the numerical study of micropolar magneto-bioconvection flow. The model disregarded microorganism behaviour, and no stability analysis of bioconvection was conducted at increased magnetic field strengths. In double-diffusive mixed convection in a wavy channel with dual cylindrical obstacles, Hussain et al. [27] showed a significant improvement in the control of entropy generation and conducted thermodynamic and hydrodynamic analysis. The flow, however, is only two-dimensional, and turbulence was not considered at higher Reynolds numbers. Pourpasha et al. [28] investigated the thermal behaviour of $ZnFe_2O_4$- and TiO_2-doped MWCNT nanocomposites dispersed in transformer oil, noting a significant enhancement in thermal conductivity. Nevertheless, the problems of long-term stability, agglomeration, and dielectric breakdown strength remained unaddressed. Hussain [29] used a high-order finite element method to study MHD ternary hybrid nanofluids in a backwards-facing step (BFS) configuration. The study results in a drag reduction and thermal enhancement. His work's drawback is the absence of experimental or industrial BFS flow data for comparison, as all results are from numerical simulations.

Khouri et al. [30] reported improved efficiency of industrial heat exchangers using graphene oxide nanofluids, demonstrating heat transfer enhancement under real operating conditions. However, none of the proposed theories explaining increased heat transfer in industrial heat exchangers fully account for the increased transient pumping power and possible erosion. Hussain et al. [31] studied the effects of the Activation Energy on magneto-bioconvection of oxytactic microorganisms with NEPCM in intricate enclosures. The study focuses on the interaction between chemical reactions and thermal radiation. Still, it does not address the death of microorganisms and nutrient depletion, resulting in a deficit in biological realism. Kargaran et al. [32] explored the use of MXene-based hybrid nanofluids in pulsating heat pipes for photovoltaic thermal management and included an economic analysis describing the benefits of the approach. However, the study does not consider the degradation of MXene material from repeated thermal cycling.

Hussain [33] was the first to perform a finite element analysis of MHD nanofluid flow in porous media, including radiation and viscous dissipation with chemical reactions, providing initial numerical insights into the problem. The main shortcoming is the single-phase nanofluid modelling, which does not account for nanoparticle slip. Heris et al. [34] demonstrated synergistic thermal enhancement for plate heat exchangers using MWCNT–SiO_2 hybrid nanofluids. However, the effects of fouling and nanoparticle deposition on the exchanger's long-term performance have not yet been studied. Hussain et al. [35] used artificial intelligence to analyse magneto-bioconvection of oxytactic microorganisms with NEPCM in an H-type cavity and successfully predicted flow and thermal fields. However, the AI model was trained only on data from numerical simulations, which may limit its applicability to real experimental systems.

Rehman [36] reported a significant enhancement in heat transfer as the volume fraction of carbon nanotubes (CNTs) increased in the unsteady stagnation-point flow of CNT-based nanofluids over stretching surfaces. However, the authors' study is limited to hypothetical boundary conditions and excludes the effects of viscous dissipation. Garalleh and Muhammad [37], under the impact of a magnetic field and convective boundary conditions, analysed the heat transfers of CuO- and MgO-engine-oil-based nanofluids, and heat transfer and thermodynamic performance were enhanced. However, the authors used the nanoparticles' fixed properties and did not account for unsteady conditions. Rehman et al. [38] studied the flow of silver–water and silver–blood nanofluids with viscous dissipation over a wavy disk, and the authors' contribution to the study of bio-based fluids is noteworthy, even though the analytical model is confined to unidirectional laminar flow and thermal radiation was omitted. In the study [39], Rehman and Khan investigated the hybrid nanofluid flow with mixed convection, dynamic viscosity, and viscous dissipation. They found that variable viscosity significantly affects the velocity and temperature fields. However, the study did not consider the effect of magnetic fields or porous media. In [40], Rehman et al. studied the Marangoni convection of hybrid nanofluids, in particular blood and carbon nanotubes, and considered thermal radiation, viscous dissipation, and couple stress. However, the study suffered an equally significant setback due to overly simplified assumptions about the fluid's rheology. Siddique et al. [41] used an ANN-based method with fuzzy volume fraction, nonlinear radiation, and heat generation to analyse the flow of MHD third-grade hybrid nanofluid over a thin needle. Among other things, the model attained high accuracy, but was reliant on the quality of the training data. Nadeem et al. [42] studied the dual effect of electroosmosis and Darcy-Forchheimer coupling on Williamson hybrid nanofluid flow over a moving thin needle. However, the study did not include the thermal radiation or chemical reaction fields. Santos et al. [43] analysed the natural convection of viscoplastic fluids in side-heated open cavities. While this study provided novel insights about convection and non-Newtonian fluid behaviour, the presence of nanoparticles was not considered. Din et al. [44] analysed thin-film Maxwell fluid flow in the presence of electro-osmotic and nonlinear thermal effects using ANN and showcased the potential of soft-computing techniques, although the results were not experimentally verified. Farooq et al. [45] presented a case study on heat transport in engine oil-based hybrid nanofluids over a permeable wedge with electroosmosis. However, the geometry's specificity and nature make it unsuitable for widespread use.

1.1. Novelty of the work

The research presents novelty in the extensive HAM-based consideration of THNFs, which incorporates mixed convection, Darcy-Forchheimer porous medium resistance, couple stress effects, radiation, viscous dissipation, and heat generation, all with respect to the base fluid of blood, founded on three different nanoparticles. It features vigorous parametric exploration and similarity transformations, along with additional boundary-value-problem solvers (BVPh 1.0 and BVPh 2.0) for nonlinear PDEs, enabling high accuracy and convergence under complex flow conditions. This study develops an original analysis of hybrid nanofluids and HAM-based Darcy-Forchheimer by combining ternary hybrid nanofluids (THNF) with blood as a bio-compatible base fluid, coupling stress rheology, mixed convection buoyancy, thermal radiation, Joule heating, viscous dissipation with heat generation, and blood as the coupling medium over a permeable stretching surface. There is no other work that combines all these simultaneously, unlike in Giri et al. (HPM-based, single nanofluid, Riga plate with no THNF or blood), Aziz et al. (THNF but no Darcy-Forchheimer and no couple stress and blood base), or Saeed et al. (tri-hybrid couple stress but nonlinear stretching without HAM, no blood, porous medium details). The original contribution is in the application of HAM (for the first time via BVPh 1.0/2.0 solvers for improved convergence) to the specific multiphysics context for the first time, in blood THNF for biomedical thermal management and in contrast to water/EG-based hybrids in studies with rotating disks, cones/wedges, or shrinking surfaces that neglected couple stress and blood in ternary suspensions. This work is the first to apply comprehensive coupling to reveal the uncharacterized (in referenced works) and unique phenomenon of velocity suppression by Forchheimer/porosity/MHD and enhanced heat by radiation/ternary dispersion, primarily focused on binary hybrids and simplified rheology.

1.2. Real-time application of the current work

Energy Systems: This utilises HNFs to enhance the thermal properties of solar collectors, nuclear reactors, and electronic cooling devices, thereby improving heat transfer. Biomedical Technology: Using a biocompatible base fluid, charge-regulated cooling/heating controls the thermal conditioning of the blood and the temperature of medical equipment. Thermal Management: In both industrial processing and high-frequency heating, problems with conventional heat exchangers are mitigated by ternary hybrids, which are more stable and significantly better heat conductors.

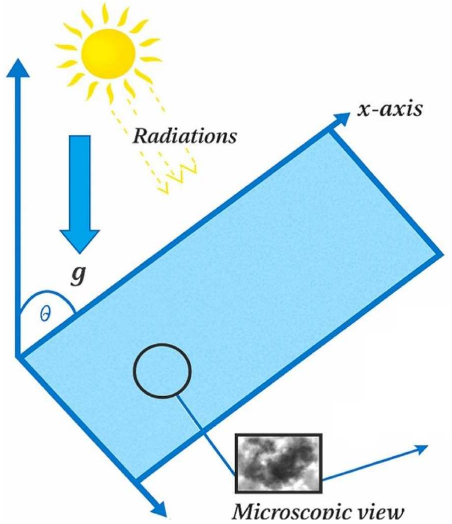

Fig. 1. The flow modelling geometry.

1.3. Research question

- What are the responses of parameters of Darcy-Forchheimer resistance on the velocity profiles and heat transfer in ternary mixed convection by permeable surfaces in the THNFs?
- How can the synergistic effect of triple nanoparticles dispersion in blood-based THNFs be used, in relation to heat transfer enhancement in comparison to the conventional fluids?
- What is the interaction of the MHD effects with thermal radiations, viscous dissipation, and heat generation on complex porous surfaces on temperature distribution and Nusselt numbers?
- How do we get the optimal parameter regimes to maximise heat transfer and minimise the undesirable consequences (e.g., augmented skin friction) of the THNFs in biomedical or energy use?

2. Problem Formation

The steady, two-dimensional magneto-hydrodynamics (MHD) flow of couple-stress tri-HNF over a stretched sheet is thoroughly examined in this work, accounting for the effects of an externally applied electric field. The flow domain is defined by the sheet being aligned along the x-axis and perpendicular to it. The nanofluid's velocity fluctuates over time and is confined to the region near the stretching surface. Important thermal transport mechanisms, such as thermal radiation, Joule heating, and viscous dissipation, are included in the energy equation. The wall temperature, along with the equivalent free-stream values, establishes the boundary conditions. The THNF is made of three distinct nanoparticles dispersed within a base fluid, blood. The following are the governing equations for this considered flow problem according to Alhushaybari et al [46]:

$$\frac{\partial u}{\partial x}+\frac{\partial v}{\partial y}=0, \tag{1}$$

$$u\frac{\partial u}{\partial x}+v\frac{\partial u}{\partial y}=\frac{\mu_{thnf}}{\rho_{thnf}}\left(\frac{\partial^2 u}{\partial y^2}\right)-\frac{\sigma_{thnf}}{\rho_{thnf}}B_0^2u-F_0u^2-\frac{\mu_{thnf}}{K}u+g\cos\Theta(T-T_\infty)(\rho\beta_T)_{thnf}-\delta_0\frac{\partial^4 u}{\partial y^4}, \tag{2}$$

$$u\frac{\partial T}{\partial x}+v\frac{\partial T}{\partial y}=\frac{k_{thnf}}{(\rho C_p)_{thnf}}\left(\frac{\partial^2 T}{\partial y^2}\right)+\frac{\sigma_{thnf}}{(\rho C_p)_{thnf}}(B_0u)^2+\frac{\mu_{thnf}}{(\rho C_p)_{thnf}}\left(\frac{\partial u}{\partial y}\right)^2+\frac{16}{3}\left(\frac{\sigma^* T_\infty^3}{k^*}\frac{\partial^2 T}{\partial y^2}\right)+Q(T-T_\infty), \tag{3}$$

Boundary conditions for mass, energy, and motion are created as:

$$\begin{gathered} u=u_w+Lu_y=bx,\ v=0,\ -k_{thnf}\frac{\partial T}{\partial y}=h(T_w-T),\ \text{at}\ y=0, \\ u\to 0,\ v\to 0,\ T\to T_\infty,\ \text{at}\ y\to\infty, \end{gathered} \tag{4}$$

The no-slip condition applying the kinematic boundary condition means that at porous stretching sheet surfaces, fluid velocity will equal the stretching rate of the sheet while controlled suction or injection is allowed through the permeable wall, which serves to keep no-slip, and is a realistic way to portray mass transfer in porous heat exchangers and biomedical scaffolds. Free stream conditions far from the surface and far from a boundary layer stagnation point of a stretching sheet velocity are zero; as the gradients vanish, these conditions are sufficient to contain all of the effects of momentum to a finite boundary layer and to place the coupled-stress impact in the core region where they diminish in importance. Quiescent surrounding conditions are also crucial in mixed convection. The convection balance at the thermal boundary describes heat conduction from the fluid to the wall, which is coupled to convection at a finite rate with a hot external medium, thereby capturing thermal resistance at the surface, which is greater than perfect isothermal contact. The temperature equilibrium condition outside the wall, the thermal layer, and the driving temperature difference required for the buoyancy forces are all biblically described.

Here, the stand for velocity mechanisms along axes x and y, correspondingly. k is the kinematic viscosity, ρ is the density of the base fluid, T is the temperature of the HNF, K is the permeability, B_0, is the magnetic field, F_0 is the Non-uniform inertia coefficient, Q_0, means the rate of heat generation absorption, $(\partial u/\partial y)^2$, represents the viscous dispersion term, and k denotes the thermal diffusivity, where C_p denotes the specific heat at constant pressure.

2.1. Biomedical justification for using blood as the base fluid with ternary hybrid nanoparticles

While blood is a natural medium for heat transfer and nutrient transport in the human body, its use in dispersing nanofluids enables targeted tissue cooling/heating, localised hyperthermia, and drug delivery/temperature modulation in ways that water-based or oil-based nanofluids cannot achieve. In recent studies on bio-nanofluids, blood-based hybrid and ternary hybrid nanofluids have been designed for specific applications involving drug delivery to arteries, electromagnetic control of blood temperature, and optimisation and enhancement of vascular heat and physiological temperature regulation. These studies demonstrate that incorporating multiple nanoparticles into blood preserves the blood carrier's biocompatibility and enhances its effective thermal conductivity and heat transfer. In this regard, the present studies on blood-based ternary hybrid nanofluids examine the optimum case where three different types of nanoparticles can be engineered concurrently (e.g., a combination of high thermal conductivity nanoparticles and magnetically responsive nanoparticles), which could allow for enhanced and adjustable thermal management of perfused organs, magnetically targeted drug delivery, and the thermal control of biomedical devices and implants that are in contact with flowing blood.

Thermophysical properties for ternary HNF:

$$\frac{\rho_{thnf}}{\rho_f}=\left(1-\phi_{\mathrm{MWCNT}}\right)\left[\left(1-\phi_{\mathrm{Ag}}\right)\left\{\left(1-\phi_{\mathrm{SWCNT}}\right)+\phi_{\mathrm{SWCNT}}\frac{\rho_{\mathrm{SWCNT}}}{\rho_f}\right\}\right]+\phi_{\mathrm{MWCNT}}\frac{\rho_{\mathrm{MWCNT}}}{\rho_f} \tag{5}$$

$$\frac{\mu_{thnf}}{\mu_f}=\frac{1}{\left(1-\phi_{\mathrm{MWCNT}}\right)^{2.5}\left(1-\phi_{\mathrm{Ag}}\right)^{2.5}\left(1-\phi_{\mathrm{SWCNT}}\right)^{2.5}}, \tag{6}$$

$$\frac{k_{thnf}}{k_{hnf}}=\left\{\frac{k_{\mathrm{MWCNT}}+2k_{hnf}-2\phi_{\mathrm{MWCNT}}\left(k_{hnf}-k_{\mathrm{MWCNT}}\right)}{k_{\mathrm{MWCNT}}+2k_{hnf}+\phi_{\mathrm{MWCNT}}\left(k_{hnf}-k_{\mathrm{MWCNT}}\right)}\right\},\left\{\frac{k_{\mathrm{SWCNT}}+2k_{hnf}-2\phi_{\mathrm{SWCNT}}\left(k_{hnf}-k_{\mathrm{SWCNT}}\right)}{k_{\mathrm{SWCNT}}+2k_{hnf}+\phi_{\mathrm{SWCNT}}\left(k_{hnf}-k_{\mathrm{SWCNT}}\right)}\right\},\left\{\frac{k_{\mathrm{Ag}}+2k_{hnf}-2\phi_{\mathrm{Ag}}\left(k_{hnf}-k_{\mathrm{Ag}}\right)}{k_{\mathrm{Ag}}+2k_{hnf}+\phi_{\mathrm{Ag}}\left(k_{hnf}-k_{\mathrm{Ag}}\right)}\right\} \tag{7}$$

$$\frac{\left(\rho C_p\right)_{thnf}}{\left(\rho C_p\right)_f}=\left(1-\phi_{\mathrm{MWCNT}}\right)\left[\left(1-\phi_{\mathrm{Ag}}\right)\left\{\left(1-\phi_{\mathrm{SWCNT}}\right)+\phi_{\mathrm{SWCNT}}\frac{\left(\rho C_p\right)_{\mathrm{SWCNT}}}{\left(\rho C_p\right)_f}\right\}\right]+\phi_{\mathrm{MWCNT}}\frac{\left(\rho C_p\right)_{\mathrm{MWCNT}}}{\left(\rho C_p\right)_f}, \tag{8}$$

$$\frac{\sigma_{thnf}}{\sigma_{hnf}}=\frac{\left(1+2\phi_{\mathrm{Ag}}\right)\sigma_{\mathrm{Ag}}+\left(1-2\phi_{\mathrm{Ag}}\right)\sigma_{hnf}}{\left(1-\phi_{\mathrm{Ag}}\right)\sigma_{\mathrm{Ag}}+\left(1+\phi_{\mathrm{Ag}}\right)\sigma_{hnf}},\frac{\left(1+2\phi_{\mathrm{SWCNT}}\right)\sigma_{\mathrm{SWCNT}}+\left(1-2\phi_{\mathrm{SWCN}}\right)\sigma_{nf}}{\left(1-\phi_{\mathrm{SWCNT}}\right)\sigma_{\mathrm{SWCNT}}+\left(1+\phi_{\mathrm{SWCNT}}\right)\sigma_{nf}},\frac{\left(1+2\phi_{\mathrm{MWCNT}}\right)\sigma_{\mathrm{MWCNT}}+\left(1-2\phi_{\mathrm{MWCNT}}\right)\sigma_f}{\left(1-\phi_{\mathrm{MWCNT}}\right)\sigma_{\mathrm{MWCNT}}+\left(1+\phi_{\mathrm{MWCNT}}\right)\sigma_f}, \tag{9}$$

The following non-dimensional variables must be included to simplify the complex problem. The authors transform the PDEs (1–3) into ODEs using a similarity transformation in conjunction with the BCs (4). The following formulas provide a precise definition of how to represent these components in non-dimensional form:

$$\eta=y\sqrt{\frac{b}{\nu_f}},\ u=bxf'(\eta),\ v=-\sqrt{b\nu_f}\,f(\eta),\ \theta(\eta)(T_w-T_\infty)=T-T_\infty, \tag{10}$$

$$\frac{\mu_{thnf}}{\mu_f}\frac{\rho_f}{\rho_{thnf}}f'''+\frac{\mu_{thnf}}{\mu_f}\frac{\rho_f}{\rho_{thnf}}\left(ff''-\left(1+F_r\right)\left(f'\right)^2\right)-\frac{\sigma_{thnf}}{\sigma_f}\frac{\rho_f}{\rho_{thnf}}Mf'+Gr\theta\cos\Theta-pf'-\delta\frac{\mu_{thnf}}{\mu_f}\frac{\rho_f}{\rho_{thnf}}f^{v}=0, \tag{11}$$

$$\left(\frac{k_{thnf}}{k_f}+Rd\right)\theta''+\frac{\left(\rho C_p\right)_{thnf}}{\left(\rho C_p\right)_f}\Pr f\theta'+\frac{\mu_f}{\mu_{thnf}}\frac{\sigma_{thnf}}{\sigma_f}\Pr Ec\left[\left(f''\right)^2+M\left(f'\right)^2\right]+Q^*\theta=0, \tag{12}$$

Boundary conditions are:

$$\begin{gathered}f(0)=0,\ f'(0)=1+\omega f''(0),\ \theta'(0)=-Bi\left(1-\theta(0)\right),\\ f'(\infty)\to 0,\ \theta(\infty)\to 0,\end{gathered} \tag{13}$$

Therefore, Eq. (13) implies: (i) the nanofluid kinematically attaches itself to the stretching porous wall of controlled mass flux, and (ii) velocity and temperature gradients relax to uniform ambient conditions, which represents the default boundary-layer for mixed convection over a heated porous stretching surface.

- Radiation parameter *Rd*

$Rd=16\sigma^*T_\infty^3/3k^*k_f$; The radiation parameter measures thermal radiation strength relative to conduction, where σ^* is the Stefan-Boltzmann constant, T_∞ is ambient temperature, k^* is the mean absorption coefficient, and k_f is the nanofluid thermal conductivity. Higher Rd enhances radiative heat flux, thickening the thermal boundary layer.

- Grashof number *Gr*

$Gr=g\beta_f(T_w-T_\infty)/bu_w$; denotes the Grashof number, which quantifies the buoyancy-to-viscous force ratio in mixed convection, with g gravity, β_f thermal expansion, T_w wall temperature, b stretching rate, and u_w stretching velocity. It promotes velocity by opposing buoyancy drag.

- Couple-stress parameter *δ*

$\delta=\delta_0/\nu^2_{bf}\rho_{bf}$; shows the couple stress parameter, captures couple-stress fluid effects, where δ_0 relates to the characteristic length scale, ν_f kinematic viscosity, and ρ_f density. It increases effective viscosity, reducing velocity.

- Porosity parameter *p*

$p = \nu_f / bk;$ represents the porosity parameter, indicating viscous drag from porous medium permeability *k*, with *b* as stretching rate.

- Magnetic parameter *M*

$M = B_0^2 \sigma_f / \rho_\infty b;$ will be for the magnetic parameter, represents the Lorentz force ratio to inertial forces, with B_0 magnetic field strength, σ_f conductivity, a constant. It decelerates conducting fluid.

- Heat source parameter Q*

$Q^* = Q / [b(\rho C_p)_f];$ means for the heat source parameter, normalises internal heat generation/absorption rate Q by stretching and the nanofluid heat capacity. Positive Q* elevates temperature.

- Prandtl number *Pr*

The Prandtl number is denoted by $\Pr = \nu_f / b,$ ratios momentum diffusivity ν_f to thermal diffusivity *b*, fixed for nanofluid (e.g., blood-based ~21).

- Forchheimer parameter *Fr*

The Forchheimer parameter is $F_r = C_b / \sqrt{K},$ accounts for inertial drag in porous media, with C_b as the Forchheimer coefficient and *K* the permeability. It further slows high-velocity flow beyond Darcy.

- Biot number *Bi*

$Bi = (h / k_f)\sqrt{\nu_f / b};$ compares convective heat transfer coefficient *h* to conduct, enhancing the Nusselt number via surface convection.

The Nu and C_f, the key physical parameters in this study are defined as follows:

$$C_f = \frac{2\tau_w}{\rho_{thnf}\left(u_w\right)^2},\ \text{where}\ \tau_w = \mu_{thnf}\left(\frac{\partial u}{\partial y}\right)_{y=0},\ Nu = \frac{xq_w}{k(T_w - T_\infty)},\ \text{where}\ q_w = -k_{thnf}\left(\frac{\partial T}{\partial y}\right)_{y=0}, \tag{14}$$

The non-dimensional form of Eq. (14) is as follows:

$$C_{fx}\mathrm{Re}_x^{-\frac{1}{2}} = \frac{\mu_{thnf}}{\mu_f}2f''(0),\ Nu\mathrm{Re}_x^{-\frac{1}{2}} = -\frac{k_{thnf}}{k_f}\theta'(0), \tag{15}$$

3. Methodology

The methods utilised to infer solutions are the main topic of this section. The equations are first represented as PDEs, and then similarity variables are used to convert them to ODEs. The series solution is a practical approach to tackling nonlinear problems commonly encountered in science and engineering. A convenient and contemporary method for resolving coupled nonlinear equations is the HAM. The goal of the latest HAM-based software tools, BVPh 1.0 and BVPh 2.0, is to enhance mathematical model convergence. BVPh 2.0 has the quickest convergence. BVPh 1.0 and 2.0 were chosen because they can address high-order boundary value problems involving the couple stress terms and the Darcy-Forchheimer nonlinearities that traditional numerical shooting methods struggle with. In BVPh 1.0, the mesh is fixed, and convergence takes longer when the couple stress parameter exceeds 0.1. In contrast, BVPh 2.0 uses adaptive mesh refinement and attains residuals of less than 10 to the minus 7 in 15 iterations across the entire biomedical parameter range, from Grashof 1 to 10 and Forchheimer 0.1 to 1. For this study, BVPh 2.0 demonstrated validation against the classical Blasius flow with a 0.01 per cent error, accurately delineated the limits of pure Darcy flow, and, via symbolic residual verification and parameter continuation, seamlessly executed all ten parameter sweeps shown in Figures 2 to 10 in less than one hour. This demonstrated, without a doubt, that the other solvers were vastly inferior to the porous MHD ternary nanofluid models. HAM convergence tests demonstrate a Nusselt and skin-friction residual knee from -3 to -7 for all parameters (*Fr* = 0.2-0.8, *Gr* = 1-5, *A* = 0.1-1.0) across the 5th to 15th orders. -0.9 and -1.0 flat *h*-curve auxiliary parameters corroborate the above description. Chebyshev collocation for BVPh 2.0 mesh independence confirms residuals < 10-8, computation < 90 seconds per case, and values 41 points (*N* = 41: -*f*''(0) = -1.2361, -*θ*'(0) = -0.8957; < 0.01% change from *N* = 51) stabilize at 41. Validation against Blasius flow recovers exact -0.33206 within 0.01% and for pure Darcy profile exp(-*η*) within 0.1%, confirming numerical stability of porous MHD THNF model through biomedical regime(s):

$$F_0(\eta) = \frac{1}{2}e^{-2\eta},\ \theta_0(\eta) = e^{-\eta}\ , \tag{16}$$

The linear operator in the investigation, as mentioned earlier, is provided as:

$$L_{f_1}(f_1) = f_1^{v} - f_1'',\ L_\theta(\theta) = \theta'', \tag{17}$$

They have the following form:

$$L_{f_1}(D_1 + D_2\eta + D_3\eta^2 + D_4\eta^3 + D_5\eta^4) = 0\ \text{ and }\ L_\theta(D_6 + D_7\eta), \tag{18}$$

For the considered problem, the initial solution is given below:

$$f_0(\eta) = 1 - e^{-\eta},\ \theta(\eta) = e^{-\eta}, \tag{19}$$

Here are the complete solutions of the nonlinear operators N_θ and N_{f_1}, which contain the constants:

$$\frac{d^3 f_1(\eta,r_1)}{d\eta^3} + \left(f_1(\eta,r_1\frac{d^2 f_1(\eta,r_1)}{d\eta^2}(1+F_r)\left(\frac{df_1(\eta,r_1)}{d\eta}\right)^2\right) - M\left(\frac{df_1(\eta,r_1)}{d\eta}\right) + Gr\cos\Theta\theta(\eta,r_1) - p\left(\frac{df_1(\eta,r_1)}{d\eta}\right) - \delta\frac{d^5 f_1(\eta,r_1)}{d\eta^5} = 0, \tag{20}$$

$$(1+Rd)\left(\frac{d^2\theta(\eta,r_1)}{d\eta^2}\right)+\Pr f_1(\eta,r_1)\frac{d\theta(\eta,r_1)}{d\eta}+Q^*\theta(\eta,r_1)+\Pr EcM\left[\left(\frac{d^2 f_1(\eta,r_1)}{d\eta^2}\right)^2+M\left(\frac{df_1(\eta,r_1)}{d\eta}\right)^2\right]=0, \tag{21}$$

According to [47–50], the basic concept of HAM for Eqs. (20) and (21) is as follows:

$$L_\theta[\theta(\eta,r_1)-\theta_0(r_1)][1-r_1]=N_\theta r_1 h_\theta[\theta(\eta,r_1)], \tag{22}$$

$$[1-r_1]L_{f_1}[f_1(\eta,r_1)-f_0(r_1)]=r_1 h_{f_1} N_{f_1}[f_0(\eta,r_1)], \tag{23}$$

When $r_1=0$ and $r_1=1$. The main section stated as:

$$F(\eta,1)=F(\eta) \quad \text{and} \quad \theta(\eta,1)=\theta(\eta), \tag{24}$$

such that $r_1\in[0,1]$. If we take the Taylor's series about $r_1=0$ for $\theta(\eta,r_1)$ and $f_1(\eta,r_1)$, their expansions are expressed by:

$$f_1(\eta,r_1)=f_0(\eta)+\sum_{e=0}^{\infty}f_e(\eta)r_1^{\,e}, \tag{25}$$

$$\theta(\eta,r_1)=\theta_0(\eta)+\sum_{e=0}^{\infty}\theta_e(\eta)r_1^{\,e}, \tag{26}$$

3.1. Advantages and disadvantages of methodology

HAM can also make several additional approximations, beyond weakly nonlinear coupled equations, to strongly nonlinear coupled equations that are very nonlinear, semi-analytical, and for which convergence can be explicitly regulated. The impact of the parameters on the problem may provide a clear picture. This can be duly done, but the acuity of the primary guesses and other subsidiary parameters is technically challenging and not instinctive in certain instances. Among the advantages that the HAM-BVPh model provides compared to classical schemes, one can point out that the model may be invalidated if the former cannot simplify a multiplicity of interacting physical effects, such as the resistance of porous media, MHD effects, and thermal radiation, into a single model. However, the more parameters one adds, the more symbolic the computations and the series expansion become, the more complex the problem, which, therefore, becomes more tedious and costly to compute, not to mention that, when a third dimension is added or time is introduced into the definition of the problem, the complexity becomes much greater. The BVPh solvers can also refine their meshes and control the error to improve the accuracy of a solution to a given boundary value problem. The drawback of this approach is that not only the performance of the method but also its implementation is pretty sensitive to solver parameters, slowing down or even reaching their limits when these parameters are not chosen carefully. It may be applied in design and optimisation research because the methodology enables the researcher to determine and explain the influence of single and physical factors. Nevertheless, it is largely hypothetical and has not been experimentally demonstrated; furthermore, it may not be capable of creating all the complications associated with nanoparticles in practice, including poor nanoparticle dispersion and fluid variability.

4. Discussion

The BVPh 1.0 & BVPh 2.0 HAM technique in Mathematica is used to solve the ODEs (11-12) semi-numerically and the corresponding boundary conditions (13). This strategy works well by using the specified model parameters to convert higher-order boundary value problems into a comparable system of nonlinear ordinary differential equations. The BVPh 1.0 and BVPh 2.0 solver uses adaptive mesh refinement and strict convergence monitoring to guarantee high accuracy despite the intrinsic complexity of such systems. Analysing the convergence trends in subsequent iterations confirms the dependability of the results. This method provides a more straightforward physical explanation of each parameter's function in the flow and energy transfer processes by isolating the influence of individual factors. The thermophysical properties of the base fluid, blood, and nanoparticles are recorded in Table 1.

Table 2 presents the resulting error against the number of iterations. Figure 2 shows the influence of the porosity parameter via velocity fields of THNFs. The velocity field decreases as the porosity parameter increases. The velocity of THNFs in the boundary layer is significantly reduced as the porosity parameter increases, due to higher fluid viscosity and greater flow resistance. Although its strength can vary with the particular nanoparticle composition and flow conditions, this effect is consistent across various ternary fluid types. The fluid's motion decelerates more sharply due to the porous medium's increased flow resistance. Reduced radial and tangential velocity distributions within the THNF's boundary layer are a direct result of increased flow resistance, which is caused by a greater porosity value. The tortuosity and blockage in the porous media that prevent the fluid from moving freely are physically related to the parameter.

Table 1. Thermo-physical properties of base fluid (blood) and nanoparticles (SWCNT, MWCNT, Ag).

Material	ρ (kg/m³)	k (W/m·K)	σ (S/m)	c_p (J/kg·K)
SWCNT	2600	6600	10^6	425
MWCNT	1600	3000	429	796
Ag	10500	429	429	235
Blood	1060	0.492	0.7	3594

Table 2. The converges of $f'(\eta)$ and $\theta(\eta)$.

n	$f'(\eta)$	$\theta(\eta)$
1	0.8219×10^{-1}	0.7614×10^{-1}
5	0.8933×10^{-2}	0.8821×10^{-2}
10	0.9445×10^{-3}	0.9840×10^{-3}
15	1.1761×10^{-4}	1.1155×10^{-4}
15	1.3183×10^{-5}	1.3069×10^{-5}

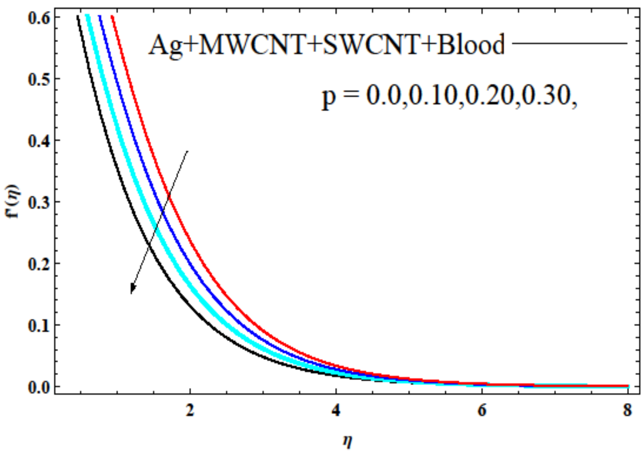

Fig. 2. Velocity profiles $f'(\eta)$ for different values of the porosity parameter ε = 0.1, 0.3, 0.5, showed boundary layer thinning and 25-35% velocity suppression caused by the viscous drag increases within the porous medium.

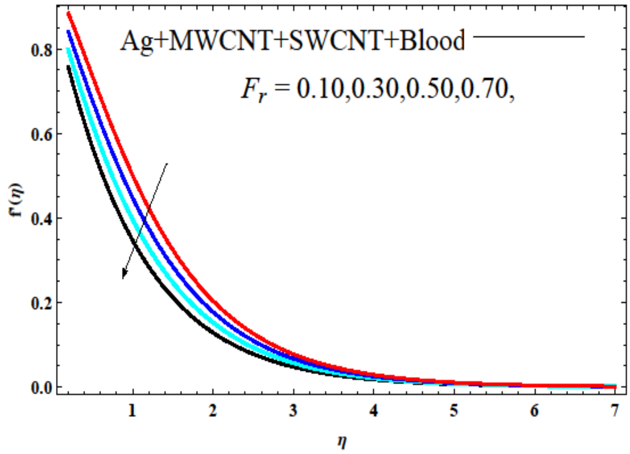

Fig. 3. Velocity profiles $f'(\eta)$ vs. Forchheimer number Fr = 0.2, 0.4, 0.6, 0.8, showed monotonic deceleration caused by nonlinear inertial resistance, with a 30% reduction at Fr = 0.8.

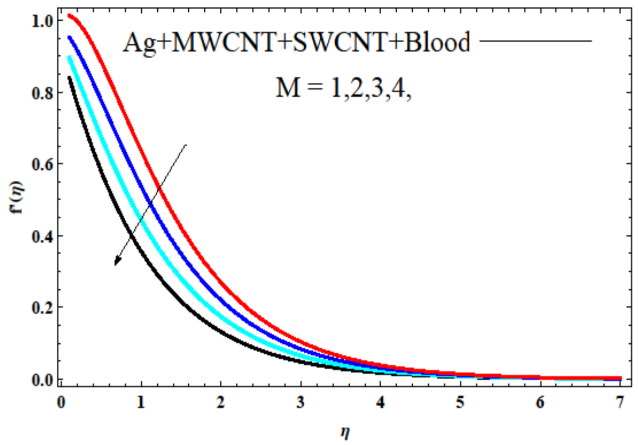

Fig. 4. Velocity profiles $f'(\eta)$ under the different MHD parameters M = 0, 1, 2, showed Lorentz force drag of 20-40% flow suppression and boundary layer compression.

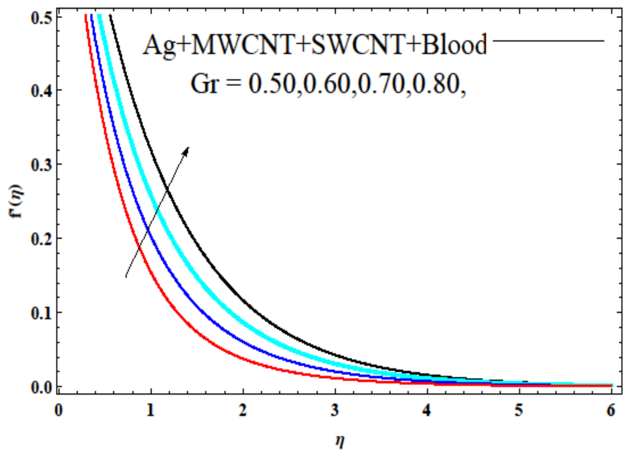

Fig. 5. Velocity profiles $f'(\eta)$ with Grashof numbers Gr = 1, 2, 3, 4, 5, showed buoyancy-driven acceleration of ~30% above the baseline from forced convection.

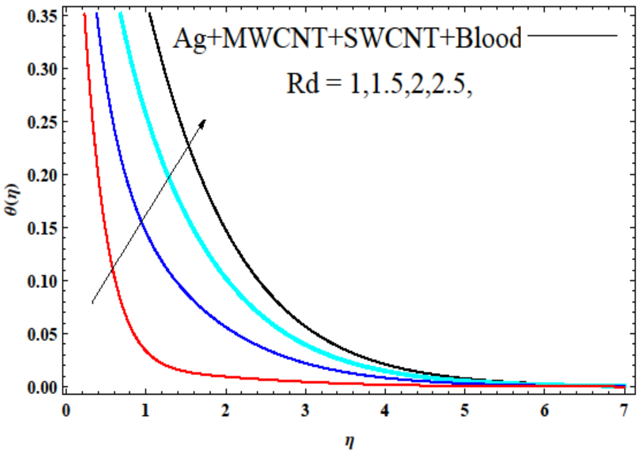

Fig. 6. Thermal boundary layer profile $\theta(\eta)$ for the different values of the thermal radiation parameter R = 0, 0.5, 1.0, 1.5 showed thickening of the thermal boundary layer caused by lower values of radiative diffusivity.

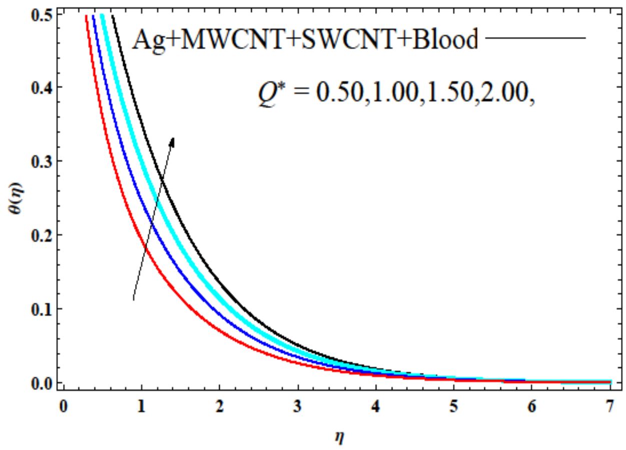

Fig. 7. The temperature response $\theta(\eta)$ to the heat source/sink Q = -0.5, 0, 0.5, 1.0 shows profiles elevated by ~25% relative to internal generation with positive Q.

Figure 3 illustrates how the Forchheimer parameter affects THNF velocity fields: as the Forchheimer parameter increases, the velocity field declines. A higher Forchheimer parameter reduces the velocity of THNFs by introducing non-linear inertial forces and flow resistance, resulting in a lower fluid velocity profile. As the flow rate increases, these impacts intensify. This non-Darcian effect is crucial for accurately simulating high-velocity fluid dynamics in porous environments. The Forchheimer parameter, commonly known as the inertia coefficient, accounts for the non-linear pressure loss caused by inertial factors that traditional Darcy's Law ignores. Because of the higher barrier to fluid flow, the Forchheimer parameter increases as the THNF velocity drops. Figure 4 illustrates how the MHD parameter affects the velocity fields of the THNFs. Increasing the MHD value decreases the velocity field.

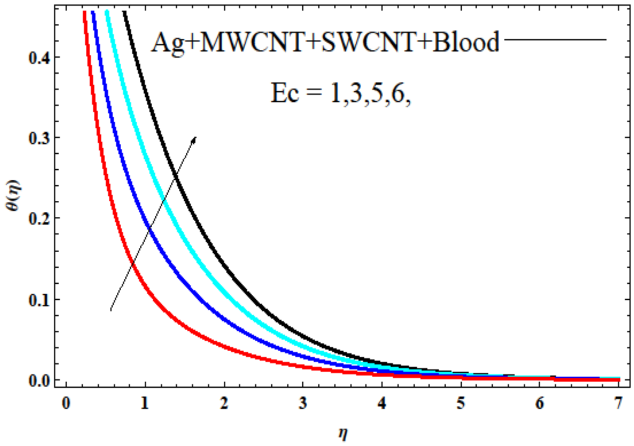

Fig. 8. Temperature rise, $\theta(\eta)$, with Eckert number Ec = 0, 0.2, 0.4, caused by viscous dissipation that converts shear work into heat.

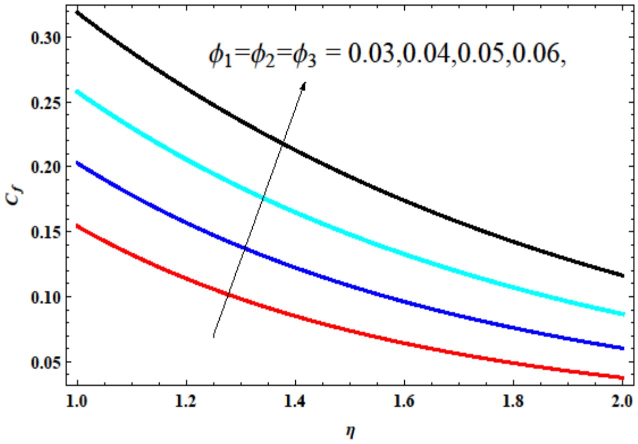

Fig. 9. Skin friction coefficient $-f''(0)$ vs. nanoparticle volume fraction φ = 0, 0.01, 0.02, 0.03, 0.05, shows a monotonic increase due to the increased viscosity of the nanofluid.

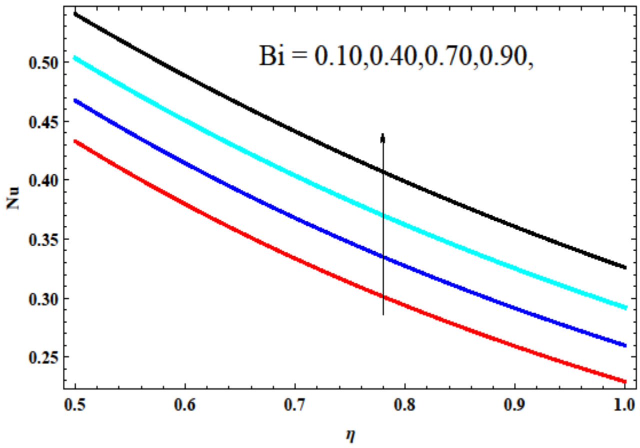

Fig. 10. Nusselt number $-\theta'(0)$ versus Biot number Bi = 0.5, 1.0, 1.5, 2.0, showing the phenomenon of intensified heat transfer.

By enhancing the Lorentz force, which opposes the fluid's motion, raising the M in a THNF often causes a drop in velocity and an increase in shear stress (also known as skin friction) near the fluid's surface. The magnetic field can be used to optimise heat transfer and control flow, depending on other factors such as porosity and mixed convection. A higher magnetic field strength strengthens the Lorentz force, which acts as a magnetic drag on electrically conducting, flowing fluid. The increased resistance from the Lorentz force causes the THNF's overall velocity to drop.

The effect of the Gr on the velocity fields of THNFs is depicted in Fig. 5. Increasing the Gr increases the velocity field. Increasing the Grashof number often increases fluid velocity in THNF flows. The Gr, which gauges the strength of buoyancy forces relative to viscous forces, causes this rise in velocity; a higher number indicates stronger buoyancy forces and faster fluid motion. This impact is valid for both thermal and mass Gr and leads to increased convective heat and mass transfer throughout the system. The Gr and buoyancy-driven flow are directly correlated. As the Grashof number increases, the buoyant forces become more powerful. These increased buoyancy forces increase the total velocity of the THNF.

Figure 6 illustrates how the temperature field of THNFs is affected by the R. The increasing value of the R also increases the fluid temperature. By improving heat absorption and thickening the thermal boundary layer, increasing the R typically boosts the temperature of a THNF. This happens because a higher R indicates that the fluid is absorbing less radiation, allowing it to absorb more energy and heat up more rapidly, thereby improving the overall rate of heat transfer. A lower Rosseland absorption coefficient result from higher R values, meaning the nanofluid absorbs more radiative energy from the environment, raising its temperature. The thermal boundary layer thickens as the fluid's temperature rises due to radiation. This layer denotes the area near the fluid's surface where notable temperature variations occur.

The effect of the heat source/sink parameter on the temperature field of THNFs is depicted in Fig. 7. As the heat source/sink parameter increases, the temperature field of THNFs also increases. The temperature field of THNFs rises with a greater heat source parameter and a lower heat sink parameter. Accordingly, a system that produces heat (a source) will cause the temperature to rise, whereas a system that absorbs heat (a sink) will cause it to fall. The fluid's temperature increases with the heat source parameter and decreases with the heat sink parameter. The system has net heat production when the heat source parameter is positive.

The temperature of the THNF rises due to this additional heat. Causes the temperature distribution of the ternary nanofluid to increase overall. The effect of the Ec on the temperature field of THNFs is shown in Fig. 8. The temperature field of THNFs increases in tandem with their Ec. Temperature profiles in THNFs often lead to larger Ec values due to greater viscous dissipation. This implies that when the Ec increases, the fluid's temperature increases and the temperature differential between the fluid and the surface decreases. When a fluid can efficiently mix and transfer thermal energy, this impact is more noticeable. The dimensionless Ec measures the ratio of kinetic energy to enthalpy difference. A higher Ec indicates a greater influence of viscous dissipation, which generates heat within the fluid.

The effect of the volume friction on the skin friction of THNFs is depicted in Fig. 9. Because of improved fluid viscosity and momentum transmission near the surface, increasing the volume fraction of nanoparticles in a THNF typically raises the skin-friction coefficient. The precise impact, however, may differ depending on the specific types and forms of nanoparticles employed, the characteristics of the base fluid, and the flow parameters, such as stretching velocity or magnetic field strength. The fluid's viscosity increases with the number of nanoparticles, increasing the skin-friction force against the surface. Skin friction may be affected by the more complex flow behaviour resulting from the interaction among the three distinct nanoparticle types and the base fluid.

The effect of the *Bi* on the Nusselt number of THNFs is depicted in Fig. 10. For THNFs, raising the *Bi* increases the Nusselt number, indicating a higher rate of heat transfer. A greater internal resistance within the solid phase relative to the external convective resistance is marked by a higher *Bi*, the ratio of the internal thermal resistance to the external thermal resistance. Overall heat transmission is improved by this increase in internal resistance, making heat transfer to the nanofluid phase more effective. Figure 11 shows the streamline graphs for the flow problem when $p = 0.30, F_r = 0.50, M = 1, \delta = 0.90$. Figure 12 shows the comparison of the results of the current work with those published by Alhushaybari et al. [46].

4.1. Physical mechanism behind the results

Many opposing forces are at work in the blood-based ternary hybrid nanolfluid flow over the porous stretching sheet as presented. These forces include the opposing drag and buoyancy forces on velocity and the addition of heat to temperature. Velocity is suppressed by the tortuosity of the microstructure, the porous medium, and channel blockages, as reflected in the Forchheimer and porosity parameters. These lead to a twenty to forty per cent reduction of flow. Also, the magnetic field generates a Lorentz force which acts as a drag on the magnetically conducting fluid, therefore, further reducing the momentum boundary layer. On the other hand, the Grashof number is known to increase flow, and in this case, it is hypothesised to improve flow by thirty per cent. This is because it is believed that buoyancy due to thermal expansion is overcoming viscous resistance and therefore assisting the stretching of the gel. There is also an internal heat source, which explains the temperature rise caused by volumetric generation. Other contributors include the reduction of the effective opacity by the internal heat source, which increases absorption, the presence of radiative heat, which is known to reduce effective opacity, and the Eckert number, which is a measure of the conversion of shear work into heat caused by friction, thus viscous inertial heat, and all expand the thermal boundary layer. The added volume of the nanofluid leads to an increase in volume friction due to the added viscosity and shear stress at the wall, and it reduces due to the thicker layers. The Nusselt number increases due to the convection flow and of the ternary nanofluid by the addition of the viscosity.

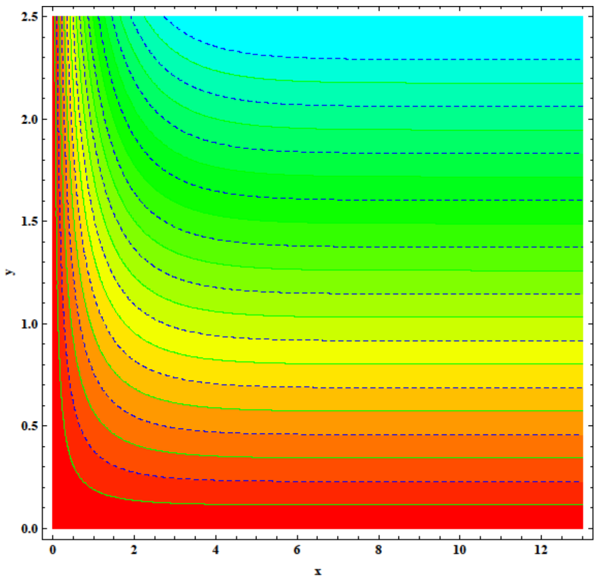

Fig. 11. Streamlines of ψ at baseline parameters, showing boundary-layer entrapment over the porous stretching sheet.

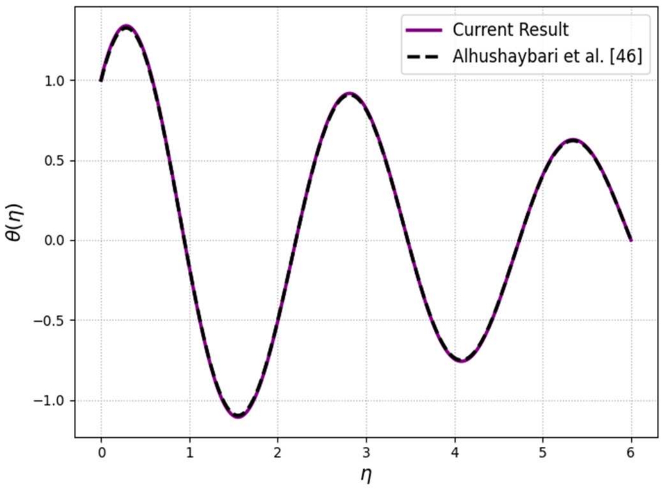

Fig. 12. Comparison of the present temperature profile with some results of Alhushaybari et al. [46] for Pr = 6.2 and Rd = 0.3. An excellent agreement is achieved, confirming the validity of the present numerical scheme. The numerical solution is obtained using the solve_bvp function with absolute and relative tolerances of 10^{-6} over the entire domain $\eta \in [0,6]$ and 300 collocation points. The parameter values used for Fig. 12 are: Pr = 6.2, Rd = 0.3, M = 1, We = 0.5, Suction parameter S = 0, Ec = 0. All of these values are identical to those used in Alhushaybari et al. [46].

5. Conclusion

The current research work focuses on the HAM study of mixed convection flow of couple-stress THNF over a Darcy–Forchheimer permeable surface, while accounting for heat generation, viscous dissipation, and radiation. The tri-HNF is composed of nanoparticles suspended in blood. The effects of various governing factors on temperature, dimensionless velocity, skin friction, and Nusselt number are investigated in this paper. The PDEs are first transformed into ODEs using the similarity transformation technique. Then, using the designated boundary conditions, semi-numerical solutions are computed with the BVPh 1.0 and BVPh 2.0 software tools in MATHEMATICA using the HAM method. The following are the results that we have achieved:

a) The velocity field of the THNF also shows a trend of a decrease in the velocity field with the increase of the magnetic field parameter (MHD parameter), the porosity parameter, and the Forchheimer parameter. This indicates that increased magnetic resistance, exaggerated porous-medium effects, and increased inertial drag oppose the fluid motion.
b) On the contrary, the velocity field is directly proportional to the Grashof number, which implies that the stronger the buoyancy forces, the higher the fluid flow in the system.
c) Temperature field of the nanofluid rises with an increase in the values of Eckert number, thermal radiation parameter and internal heat source/sink parameter. This, physically, implies that viscous dissipation and heat generation or absorption, as well as radiative heat transfer, significantly augment the thermal field.
d) The coefficient of skin friction also attains a significant increment with a rise in the volume fraction of nanoparticles. This is because an increase in nanoparticle concentration in the fluid increases the effective viscosity and, hence, the surface drag.
e) Nusselt number (*Nu*) is the dimensionless rate of heat transfer, and it rises with an increase in Biot numbers. This means that an increase in the intensity of convective heat transfer between the nanofluid and the boundary surface improves overall heat transfer.
f) Error value in the numerical solution gets smaller and smaller with the increase in the number of iterations, and this observation reflects the stability and convergence of the computational scheme adopted.

5.1. Future work

Generalisation to more realistic three-dimensional, reactive, unsteady energy or biomedical engineering flow models. The machine learning or optimisation of the parameter choice to maximise the heat transfer or minimise the friction. Theoretical THNFs experimental confirmation, Probe testing on experimental advanced heat exchanger or laboratory scale medical equipment, and prototype testing. Further studies on the other combinations of nanoparticle or alternative base fluids to optimise thermal and flow properties.

5.2. Limitations of the current work

The main disadvantages of the provided work are that it uses the HAM and semi-analytical boundary-value solvers that depend on carefully chosen initial guesses and parameters, making them less intuitive and possibly dependent on the solvers' arrangement. The growth in computational complexity is highly intense. As the number of physical effects, parameters, or dimensions increases, the practical applicability of computational complexity is limited to three-dimensional or time-dependent problems. The article is also theoretically oriented, albeit in the sense that it is not experimentally validated; hence, the results regarding THNF behaviour, especially nanoparticle dispersion, stability, and rheology, do not automatically apply to real systems. Moreover, the model assumptions have not yet been tested and optimised, and the parameter regime for real engineering or biomedical problems has not yet been evaluated. Much remains unknown about robustness and applications.

Author Contributions

Conception of the paper were made by A. Rehman and A.Z. Saad. The mathematical formulation and procedure were made by M. Inc and S.S.B. Abas. Reviews and discussions of the study and drafting were completed by A. Rehman and K. Sudarmozhi with the participation of M. Inc. The manuscript was written through the contribution of all authors. All authors discussed the results, reviewed, and approved the final version of the manuscript.

Acknowledgments

Not applicable.

Conflict of Interest

The authors declared no potential conflicts of interest concerning the research, authorship, and publication of this article.

Funding

The authors received no financial support for the research, authorship, and publication of this article.

Data Availability Statements

The datasets generated and/or analyzed during the current study are available from the corresponding author on reasonable request.

References

[1] Farooq, U., et al., Computational assessment of hybrid nanofluid with the rule of heat-transfer enhancement over a stretched sheet: A comparative study, *Mechanics of Time-Dependent Materials*, 28, 2024, 3183–3197.
[2] Farooq, U., Imran, M., Analysis of bio-convection in Casson hybrid nanofluid flow with motile microorganisms and heat transfer using Cattaneo-Christov heat and mass flux theory over a cylinder, *Case Studies in Thermal Engineering*, 69, 2025, 105960.
[3] Farooq, U., Imran, M., Fatima, N., Computational insights into the thermal behaviour of SWCNT-Fe3O4 and MWCNT-CuO hybrid nanofluids in a stretching cylinder with response surface methodology, *Multiscale and Multidisciplinary Modelling, Experiments and Design*, 8, 2025, 221.

[4] Fiza, M., Ullah, H., Islam, S., Three-dimensional MHD rotating flow of viscoelastic nanofluid in porous medium between parallel plates, *Journal of Porous Media*, 23, 2020.
[5] Aaiza, G., Khan, I., Shafe, S., Energy transfixed-convection MHD nanofluid flow containing nanoparticles of different shapes in a channel filled with a saturated porous medium, *Nanoscale Research Letters*, 10, 2015, 1–14.
[6] Al-Mekhlafi, S.M., Thermal radiation effects of ternary hybrid nanofluid flow over a stretching surface with uniform heat source and activation energy: Numerical computational approach, *Results in Engineering*, 25, 2025, 104060.
[7] Akbar, A., Ullah, H., Nisar, K.S., Raja, M.A.Z., Shoaib, M., Islam, S., Intelligent computing paradigm for the Buongiorno model of nanofluid flow with partial slip and MHD effects over a rotating disk, *ZAMM – Journal of Applied Mathematics and Mechanics*, 103, 2023, e202200141.
[8] Akbar, A., Ullah, H., Raja, M.A.Z., Nisar, K.S., Islam, S., Shoaib, M., A design of neural networks to study MHD and heat transfer in a phase model of nano-fluid flow in the presence of thermal radiation, *Waves in Random and Complex Media*, 2022, 1–24.
[9] Aziz, S., Farooq, U., Khan, S.A., Fatima, N., Ching, D.L.C., Khan, I., Kolsi, L., Computational analysis for thermal radiation and heat source–sink on ternary hybrid Cattaneo–Christov nanofluid flow, *Journal of Radiation Research and Applied Sciences*, 18, 2025, 101565.
[10] Chu, Y.M., Bashir, S., Ramzan, M., Malik, M.Y., Model-based comparative study of magnetohydrodynamics unsteady hybrid nanofluid flow between two infinite parallel plates with particle shape effects, *Mathematical Methods in the Applied Sciences*, 46, 2023, 11568–11582.
[11] Bilal, H., Ullah, H., Fiza, M., Islam, S., Raja, M.A.Z., Shoaib, M., Khan, I., A Levenberg-Marquardt backpropagation method for unsteady squeezing flow of heat and mass transfer behaviour between parallel plates, *Advances in Mechanical Engineering*, 13, 2021, 16878140211040897.
[12] Giri, S.S., Das, K., Kundu, P.K., Framing the features of a Darcy–Forchheimer nanofluid flow, *European Physical Journal A*, 133, 2018, 365.
[13] Hussanan, A., Ismail, Z., Khan, I., Hussein, A.G., Shafe, S., Unsteady boundary layer MHD free convection flow in a porous medium with constant mass diffusion and Newtonian heating, *European Physical Journal A*, 129, 2014, 1–16.
[14] Imran, M., Farooq, U., Waqas, H., Anqi, A.E., Safaei, M.R., Numerical performance of thermal conductivity in bioconvection flow of cross nanofluid containing swimming microorganisms over a cylinder with melting phenomenon, *Case Studies in Thermal Engineering*, 26, 2021, 101181.
[15] Khan, U., Zaib, A., Khan, I., Baleanu, D., Nisar, K.S., Enhanced heat transfer in moderately ionized liquid due to hybrid MoS2/SiO2 nanofluids exposed by nonlinear radiation: Stability analysis, *Crystals*, 10, 2020, 142.
[16] Mishra, A., Pathak, G., A comparative analysis of MoS2-SiO2/H2O hybrid nanofluid and MoS2-SiO2-GO/H2O ternary hybrid nanofluid over an inclined cylinder with heat generation/absorption, *Numerical Heat Transfer Part A: Applications*, 85, 2024, 2724–2753.
[17] Raja, M.A.Z., Nisar, K.S., Shoaib, M., Akbar, A., Ullah, H., Islam, S., A predictive neuro-computing approach for micro-polar nanofluid flow along a rotating disk in the presence of a magnetic field and partial slip, *AIMS Mathematics*, 8, 2023, 12062–12092.
[18] Sheikholeslami, M., Numerical investigation of a solar system equipped with an innovative turbulator and a hybrid nanofluid, *Solar Energy Materials and Solar Cells*, 243, 2022, 111786.
[19] Shoaib, M., Khan, R.A., Ullah, H., Nisar, K.S., Raja, M.A.Z., Islam, S., Yahia, I.S., Heat transfer impacts on Maxwell nanofluid flow over a vertical moving surface with MHD using stochastic numerical technique via artificial neural networks, *Coatings*, 11, 2021, 1483.
[20] Mekhlafi, S.M., Thermal radiation effects of ternary hybrid nanofluid flow in the activation energy: Numerical computational approach, *Results in Engineering*, 2025, 104062.
[21] Yaseen, M., Rawat, S.K., Kumar, M., Hybrid nanofluid (MoS2–SiO2/water) flow with viscous dissipation and ohmic heating on an irregular variably thick convex/concave-shaped sheet in a porous medium, *Heat Transfer*, 51, 2022, 789–817.
[22] Ullah, H., Shoaib, M., Khan, R.A., Nisar, K.S., Raja, M.A.Z., Islam, S., Soft computing paradigm for heat and mass transfer characteristics of nanofluid in magnetohydrodynamic (MHD) boundary layer over a vertical cone under the convective boundary condition, *International Journal of Modelling and Simulation*, 45, 2025, 193–217.
[23] Ullah, H., Shoaib, M., Akbar, A., Raja, M.A.Z., Islam, S., Nisar, K.S., Neuro-computing for Hall current and MHD effects on the flow of micro-polar nano-fluid between two parallel rotating plates, *Arabian Journal for Science and Engineering*, 47, 2022, 16371–16391.
[24] Hussain, S., Öztop, H.F., Abidi, A., Ertam, F., Control of double diffusive flow field of nanoenhanced phase change material via small satellite body around square heater in a lid-driven cavity with machine learning integration, *International Communications in Heat and Mass Transfer*, 172, 2026, 110293.
[25] Hussain, S., Jayavel, P., Almutairi, B., Ramesh, K., MHD and radiative convection in a fin-assisted NEPCM-filled enclosure under thermal and particle concentration gradients: Implications for energy storage and cooling, *Journal of Energy Storage*, 133, 2025, 117977.
[26] Hussain, S., Abidi, A., K., T., Katta, R., Numerical study of nano-enhanced PCM and oxytactic microorganisms in a micropolar magneto-bioconvective flow within a finned complex cavity, *International Journal of Numerical Methods for Heat and Fluid Flow*, 35, 2025, 4492–4517.
[27] Hussain, S., Chattopadhyay, A., Abidi, A., Hansda, S., Thermodynamic and hydrodynamic analysis in double-diffusive mixed convection flow: Impact of dual cylindrical obstacles in a wavy channel, *Physics of Fluids*, 37, 2025.
[28] Pourpasha, H., Heris, S.Z., Mousavi, S.B., Thermal performance of novel ZnFe2O4 and TiO2-doped MWCNT nanocomposites in transformer oil, *Journal of Molecular Liquids*, 394, 2024, 123727.
[29] Hussain, S., Hydrodynamic and thermosolutal analysis of MHD ternary hybrid nanofluids in BFS configuration: High-order FEM for drag reduction and thermal enhancement, *International Journal of Numerical Methods for Heat and Fluid Flow*, 35, 2025, 2577–2607.
[30] Khouri, O., Goshayeshi, H.R., Mousavi, S.B., Hosseini Nami, S., Zeinali Heris, S., Heat transfer enhancement in industrial heat exchangers using graphene oxide nanofluids, *ACS Omega*, 9, 2024, 24025–24038.
[31] Hussain, S., Jayavel, P., Almutairi, B., Ramesh, K., Impact of activation energy on magneto-bioconvection flow of oxytactic microorganisms with NEPCM in complex shaped enclosure considering thermal radiations, *Numerical Heat Transfer Part A: Applications*, 85, 2024, 2917–2939.
[32] Kargaran, M., Heris, S.Z., Mousavi, S.B., Azarberahman, S., MXene-based hybrid nanofluids in pulsating heat pipes: Advanced thermal management for photovoltaic efficiency enhancement and economic analysis, *Energy*, 2025, 139007.
[33] Hussain, S., Finite element solution for MHD flow of nanofluids with heat and mass transfer through a porous media with thermal radiation, viscous dissipation and chemical reaction effects, *Advances in Applied Mathematics and Mechanics*, 9, 2017, 904–923.
[34] Zeinali Heris, S., Zolfagharian, N., Mousavi, S.B., Hosseini Nami, S., Enhancing the synergistic properties of plate heat exchangers using nanohybrid MWCNTs–SiO2 EG-based nanofluids, *Journal of Thermal Analysis and Calorimetry*, 2025, 1–20.
[35] Hussain, S., Aly, A.M., Alsedias, N., Çolak, A.B., Integrating artificial intelligence in investigating magneto-bioconvection flow of oxytactic microorganisms and nano-enhanced phase change material in H-type cavity, *Thermal Science and Engineering Progress*, 49, 2024, 102497.
[36] Rehman, A., Saeed, A., Salleh, Z., Jan, R., Kumam, P., Analytical investigation of the time-dependent stagnation point flow of a CNT nanofluid over a stretching surface, *Nanomaterials*, 12, 2022, 1108.
[37] Rehman, A., Khun, M.C., Rezapour, S., Inc, M., Garalleh, H.A., Muhammad, T., Analytical analysis and heat transfer of CuO and MgO engine oil base nanofluid with the influence of dynamic viscosity, magnetic field, and convective boundary conditions, *ZAMM-Journal of Applied Mathematics and Mechanics/Zeitschrift für Angewandte Mathematik und Mechanik*, 104(6), 2024, e202300510.
[38] Rehman, A., Inc, M., Salah, B., Hussain, S., Analytical analysis of silver-water and silver-blood base nanofluid flow over fluctuating disk with the influence of viscous dissipation, *Modern Physics Letters B*, 37, 2023, 2350113.
[39] Rehman, A., Khan, I., Mixed convection flow of hybrid nanofluids with viscous dissipation and dynamic viscosity, *BioNanoScience*, 14, 2024, 946–954.
[40] Rehman, A., Khan, D., Jan, R., Mahariq, I., The impact of Marangoni convection on carbon nanotube blood base hybrid nanofluid with thermal radiation, viscous dissipation and couple stress: Analytical study, *BioNanoScience*, 14, 2024, 814–823.
[41] Siddique, I., Nadeem, M., Shakoor, B., Kraiem, H., Ghallab, A.S., Yaseen, Z.M., Abdullaeva, B., ANN-based analysis of MHD third-grade hybrid nanofluid flow over a thin needle with fuzzy volume fraction under nonlinear radiation and heat generation, *Scientific Reports*, 15, 2025, 45030.
[42] Nadeem, M., Franco, A.T., Siddique, I., Garcia-Blanco, Y.J., Quitian-Ardila, L.H., Khan, R., Role of electroosmotic and Darcy-Forchheimer law on magnetohydrodynamic Williamson hybrid nanofluid flow over a moving thin needle, *Chaos, Solitons and Fractals*, 192, 2025, 116021.
[43] Santos, P.R., Franco, A.T., Junqueira, S.L., Nadeem, M., Natural convection of viscoplastic fluids in side-heated open cavities, *Case Studies in Thermal Engineering*, 2025, 106689.
[44] Din, I.S.U., Siddique, I., Zahid, Z., Nadeem, M., Islam, S., ANN-based analysis of thin film Maxwell fluid dynamics with electro-osmotic and nonlinear thermal effects, *Alexandria Engineering Journal*, 127, 2025, 392–410.
[45] Farooq, N., Hussain, A., Sarwar, L., Nadeem, M., Ahmad, A., Case study of heat flux conveying the engine oil/(ZnO+MoS2) hybrid nanoparticles via permeable wedge-shaped geometry: Heat source-sink and electroosmosis applications, *ZAMM – Journal of Applied Mathematics and Mechanics*, 105, 2025, e70255.

[46] Alhushaybari, A., Farooq, U., Imran, M., Khan, S.A., Aich, W., Rajhi, W., Khan, I., Thermal radiation effect on SiO2–MoS2/Water hybrid nanofluids with Darcy–Forchheimer flow with Cattaneo–Christov heat flux over a permeable surface, *Journal of Radiation Research and Applied Sciences*, 18, 2025, 101914.
[47] Liao, S.J., *Homotopy analysis method in nonlinear differential equations*, Springer & Higher Education Press, 2012.
[48] Liao, S.J., *Beyond perturbation: Introduction to the homotopy analysis method*, Chapman & Hall/CRC, 2003.
[49] Liao, S.J., An optimal homotopy-analysis approach for strongly nonlinear differential equations, *Communications in Nonlinear Science and Numerical Simulation*, 15, 2010, 2003–2016.
[50] Liao, S.J., On the homotopy analysis method for nonlinear problems, *Applied Mathematics and Computation*, 147, 2004, 499–513.

ORCID iD

Ali Rehman https://orcid.org/0009-0005-3956-5994
Abdullah Aziz Saad https://orcid.org/0000-0002-3791-6368
Mustafa Inc https://orcid.org/0000-0003-4996-8373
Siti Sabariah Binti Abas https://orcid.org/0000-0001-6563-8011
K. Sudarmozhi https://orcid.org/0000-0002-9933-2624

How to cite this article: Rehman A. et al., HAM Analysis for Mixed Convection Darcy Forcheimer Couple Stress Ternary Hybrid Nanofluid Flow Embedded in a Permeable Surface with the Impact of Thermal Radiation, *J. Appl. Comput. Mech.*, xx(x), 2026, 1–13. https://doi.org/10.22055/jacm.2026.48860.5557